Phonon dispersion curves for ordered, partially-ordered and disordered iron-aluminium alloys



1991 J. Phys.: Condens. Matter 3 8181

(http://iopscience.iop.org/0953-8984/3/42/013)

J. Phys.: Condens. Matter 3 (1991) 8181–8194. Printed in the UK

# Phonon dispersion curves for ordered, partially-ordered and disordered iron–aluminium alloys

I M Robertson†
Department of Metallurgy, University of Newcastle, Australia

Received 29 October 1990, in final form 1 July 1991

**Abstract.** Neutron inelastic scattering determination of the phonon dispersion curves in high symmetry directions for iron–aluminium alloys are presented. The alloys have compositions near 25 atomic percent aluminium, and were prepared in three states of ordered BCC, B2 and $D0_3$ structures. The data were analysed by fitting sixth-nearest neighbour Born–von Karman models. The phonon frequencies follow a consistent trend in the ordering sequence BCC to B2 to $D0_3$. A similar trend is apparent in the values of the atomic force constants for the nearest neighbours but is less apparent for the force constants for more distant nieghbours. Of the low frequency modes, the soft [$qq0$] transverse mode is the most sensitive to changes in the atomic force constants. High frequency modes exhibit large changes in frequency as a result of ordering because of the large difference in the masses of iron and aluminium atoms, as well as the changes in force constants.

## 1. Introduction

In this study, phonon dispersion curves have been determined for iron–aluminium alloys with compositions close to $Fe_3Al$ in three states of order: BCC (disordered), B2 (partially ordered) and $D0_3$ (almost fully ordered). A preliminary report has already been published (Robertson 1985). Van Dijk (1970) obtained an almost complete set of results for $D0_3$-ordered $Fe_3Al$ but did not examine the other states of order. The lattice dynamics of a number of disordered alloys have been examined previously (see for example Nicklow 1979, Venkataraman *et al* 1975) but only in the case of $Cu_3Au$ (Hallman 1974, 1976) and FeCo (Vasil'kevich 1981) have ordered and disordered alloys been compared.

For FeCo, ordering is claimed not to alter the phonon spectrum, but it is doubtful that complete disorder can be quenched-in for FeCo in the form of the large single cyrstals necessary for inelastic neutron scattering measurements (Smith and Rawlings 1976). In the case of $Cu_3Au$, changes in the dispersion curves on ordering could be accounted for by a simple second-nearest neighbour Born–von Karman model using the (mass-adjusted) interatomic force constants for pure copper.

Iron–aluminium was chosen for the present study because of the ability to obtain three distinct states of order by simple heat treatment, the retention of cubic symmetry and satisfactory neutron scattering/absorption properties.

† Present address: Materials Division—MRL, PO Box 50, Ascot Vale 3032, Australia.

0953-8984/91/428181+14$03.50  

The changes to dispersion curves that can be expected simply as a result of the symmetry change on ordering (Brockhouse 1966) may be summarized as follows:

(i) Development of gaps at the Brillouin zone boundaries of the ordered structure (ordering reduces the size of the Brillouin zone).

(ii) Occurrence of optic modes.

(iii) Splitting of formerly degenerate modes, and at points where modes which belong to the same representation repel each other.

Some of these expected changes are apparent in the dispersion curves for B2-ordered CuZn (Gilat and Dolling 1965) and $D0_3$-ordered $Fe_3Al$ (van Dijk 1970). Together with $Cu_3Au$, FeCo and $CuZn_2Al$ (Robinson *et al* 1984) these appear to be the only ordered alloys for which data are available.

More data are available on the changes in elastic constants due to ordering. For $Cu_3Au$ and $Ni_3Fe$ there are minor changes in the single-crystal elastic constants on ordering (Flinn *et al* 1960, Turchi *et al* 1978). Owen (1990) presented data for $Fe_3Pt$ in different states of order, and Castan *et al* (1990) considered the elastic constants of $A_3B$ alloys from a theoretical viewpoint. Elastic constants are available for $Fe_3Al$ only in the $D0_3$ form (Leamy *et al* 1967).

Order–disorder transitions in Fe–Al alloys with about 25 atomic percent aluminium have been studied in some detail. The high-temperature disordered BCC phase can transform to either the B2 or the $D0_3$ structure on cooling depending on composition and cooling rate.

Bradley and Jay (1932) and Taylor and Jones (1958) used powder x-ray diffraction to show that with less than 25 at.% aluminium it is possible to quench-in the disordered state. Subsequent work by Oki *et al* (1973a) indicates that the aluminium content must be below 23 at.% in order to retain disorder to room temperature. At higher aluminium contents, quenching results in a high degree of (but not complete) B2 order. Swann *et al* (1972), using transmission electron microscopy, and Guttman *et al* (1969), from single-crystal x-ray work, claim that the BCC to B2 transition is second order.

Low-temperature annealing results in the gradual development of the $D0_3$ structure for all compositions near 25 at.% aluminium (Bradley and Jay 1932). The kinetics have been studied by Okamoto and Beck (1971) and Oki *et al* (1973a, 1973b, 1977). Phase diagrams have been published by Swann *et al* (1972), Okamoto and Beck (1971) and Koster and Godecke(1980).

In the B2 structure, the BCC lattice is divided into two sublattices. Iron atoms occupy the cube corner positions and the body-centre positions are occupied by a mixture of iron and aluminium atoms.

The cubic $D0_3$ structure is also based on the BCC structure, but the conventional unit cell contains eight BCC cells and the lattice parameter is doubled. The BCC lattice is divided into four FCC sublattices, three of which are occupied by iron atoms and the other by aluminium. Defining '$a$' as the BCC lattice parameter (and $A = 2a$ as $D0_3$ lattice parameter), the sublattices are identified as follows:

| | | |
|---|---|---|
| Sublattice 1 | Fe at (000) | + FCC translations such as $(110)a$. |
| Sublattice 2 | Fe at $(100)a$ | |
| Sublattice 3 | Fe at $(111)a/2$ | |
| Sublattice 4 | Al at $(311)a/2$ | |

Sublattices 1 and 2 are crystallographically equivalent. The $D0_3$ structure represents a

further ordering of the B2 structure in which the B2 body-centre sublattice is divided into two distinct sublattices.

Figure 1 depicts a {110} section through reciprocal space for the BCC, B2 and $D0_3$ structures with relative lattice parameters applicable to the phases of the Fe–Al system. Note the progressive reduction in size of the Brillouin zone as a result of ordering.

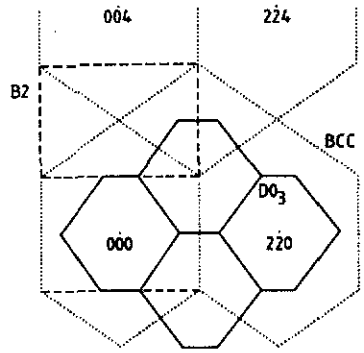


**Figure 1.** BCC (dotted lines), B2 (dashed lines) and $D0_3$ (full lines) Brillouin zone boundaries in a {110} section through reciprocal space. The relative lattice parameters are appropriate to structures formed by Fe–Al alloys. Indexing is appropriate to $D0_3$ (halve the indices for BCC and B2).

## 2. Experimental procedure

Details of the experimental procedure have been reported elsewhere (Robertson 1985). Inelastic neutron scattering measurements were performed with the triple-axis spectrometer at the Australian Nuclear Science and Technology Organization's HIFAR reactor by the constant $Q$ method. Measurements were confined to high symmetry directions $[00q]$, $[qq0]$ and $[qqq]$ in the $D0_3$ case, and also some corresponding zone boundary modes for the B2 and BCC crystals.

Some initial measurements on the B2 crystal were performed using the (111) reflection from the copper monochromator crystal. It was found that the resulting resolution was probably insufficient to reveal zone boundary splittings of the magnitude observed by van Dijk (1970) for $Fe_3Al$. For all subsequent scans the spectrometer was operated with the monochromator set for reflection from the (113) planes. This reduced the half width of equivalent neutron groups by a factor of about 0.7.

Single crystals of Fe–Al were grown by the Bridgman method and heat treated to obtain the types of ordering shown below:

| | |
|---|---|
| Fe—22.5 at.% Al | BCC (disordered) |
| Fe—25 at.% Al | $B^2$ |
| Fe—25 at.% Al | $D0_3$ |

The composition of the BCC crystal was adjusted to 22.5 at.% aluminium in order to be able to quench in the BCC structure. This was considered to a more satisfactory procedure than making high temperature measurements on an Fe–25 at.% Al crystal.

The B2 crystal was quenched from 800 °C. The work of Oki *et al* (1973a) shows that this results in B2 order with an order parameter of

$$S_{11} = 2(f_{Al} - \alpha) = 0.20$$

where $f_{Al} = 0.25$ is the fraction of aluminium in the alloy and $\alpha = 0.15$ is the fraction of aluminium atoms on the iron sublattice. The $D0_3$ crystal was annealed for a total of 500 hours at temperatures of about 400 °C. The results of Okamoto and Beck (1971) show that this results in $D0_3$ order parameters of

$$S_{11} = 0.47$$
$$S_{31} = \gamma - \beta = 0.83$$

where $\beta$ and $\gamma$ are the fractions of aluminium atoms on sublattices 3 and 4 respectively (Rudman 1960). These values were checked approximately by measuring fundamental and superlattice Bragg intensities with the triple-axis spectrometer. Born–von Karman phonon dispersion curves are not very sensitive to the exact degree of order except for the highest frequency modes.

## 3. Lattice dynamics of the $D0_3$ structure

The experimental phonon frequency data obtained in the present study were analysed by fitting Born–von Karman models. Solutions of the dynamical equations have been published for the $D0_3$ structure up to second-nearest neighbours (Borgonovi *et al* 1967), for the B2 structure up to fifth neighbours (Gilat and Dolling 1965) and for the BCC structure up to eighth neighbours (Brockhouse *et al* 1967). As part of the present work, the dynamical equations were solved for the $D0_3$ structure up to sixth-nearest neighbours (which also encompasses B2 and BCC cases).

The atomic force constant (AFC) matrices have the same form for all three structures, but for the B2 and $D0_3$ cases the matrices for a particular neighbour rank are not unique. For example, $D0_3$ nearest neighbour pairs can be Fe–Fe or Fe–Al, and B2 second neighbours can be Fe–Fe or Fe/Al–Fe/Al.

The notation for the AFCs used here is a modification of that used by Brockhouse *et al* (1967) for the BCC lattice, and takes the form $\sigma i^{nm}$ where $\sigma$ signifies a unique component of the matrix, $i$ is the rank of the neighbour atom, and $n$ and $m$ identify the sublattices of the pair of atoms involved. (For B2 order the cube corner sublattice is denoted 1 and the body centre 3 for the consistency with the $D0_3$ sublattice numbering above.) The order of $n$ and $m$ is unimportant.

## 4. Results

Experimental data points from the present work are listed in tables 1, 2 and 3 and compared in figure 2. The figure also incorporates some of van Dijk's (1970) data for high frequency modes in the $D0_3$ structure. For phonon frequencies below 8 THz the differences between the three sets of curves are small, and in almost all cases the B2 data points lie between the corresponding BCC and $D0_3$ curves. However, the high frequency modes in $D0_3$ are at about 10 THz, compared with frequencies of about

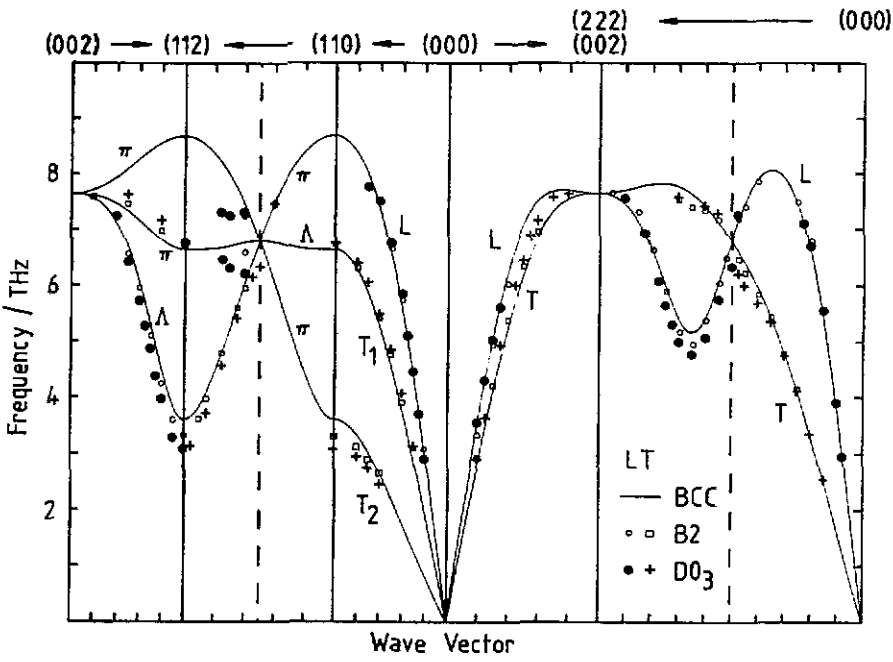


**Figure 2.** Comparison of experimental phonon dispersion curves for BCC, B2 and $D0_3$ ordered Fe–Al ($D0_3$ indexing). All data points below 8 THz were obtained in the present study. Those above 8 THz are from van Dijk (1970).

8 THz for the corresponding BCC modes. This is probably the strongest effect of ordering. The high frequency modes have eigenvectors in which predominantly the aluminium sublattice oscillates.

For the $D0_3$ structure, the more complete set of data determined by van Dijk (1970) is in very good agreement with the present results. The only significant exception is the $[00q]$ $\Delta_2'$ and $\Delta_1^{(2)}$ modes (van Dijk's notation) which derive from the degenerate BCC $[\frac{1}{2}\frac{1}{2}\frac{1}{2}]$ Λ mode. The present data show a wider separation of these modes than van Dijk's data (1970). This difference is possibly due to differences in the exact degree of $D0_3$ order for the different crystals. The degree of $D0_3$ order is also expected to have a large effect on the frequencies of the phonons at frequencies of about 10 THz.

Van Dijk's data have been analysed here using the sixth-neighbour Born–von Karman model mentioned above. However they have not been combined with the present $D0_3$ results because we desired to maintain a direct comparison between BCC, B2 and $D0_3$ results obtained under identical conditions. The measured positions of the dispersion curves depend to some extent on the resolution of the spectrometer. Incorporation of the van Dijk data for just one of the ordered states would mask the changes due to the different states of order (the main object of the present work).

The qualitative differences between the dispersion curves for the three states of order are discussed first. The quantitative differences are then described with reference to the atomic force constants (AFC) obtained by least squares curve fitting to Born–von Karman models. The phonon modes are described in terms of the $D0_3$ wave vector

**Table 1.** Frequencies in THz ($\nu$) of [00$q$] $D0_3$ modes and corresponding [00$q$] and [11$q$] B2 and BCC modes. The wave vector $q$ is in units of $2\pi/A$ where $A$ is the $D0_3$ lattice parameter. Errors (in THz) are 0.1 to 0.2 of FWHM of neutron groups. Ruled lines are at positions of $D0_3$ origin or zone boundaries.

| | BCC | | B2 | | $D0_3$ | | BCC–$D0_3$ |
|---|---|---|---|---|---|---|---|
| $q$ | $\nu$ | Error | $\nu$ | Error | $\nu$ | Error | |
| Longitudinal | | | | | | | |
| 0.40 | 3.42 | 0.14 | 3.33 | 0.13 | 3.55 | 0.09 | −0.13 |
| 0.50 | 4.42 | 0.14 | — | — | 4.30 | 0.15 | 0.12 |
| 0.60 | 5.00 | 0.14 | 4.93 | 0.06 | 5.03 | 0.08 | −0.03 |
| 0.70 | — | — | — | — | 5.60 | 0.12 | — |
| 0.80 | 6.10 | 0.07 | 6.02 | 0.07 | — | — | — |
| 0.90 | 6.59 | 0.10 | — | — | — | — | — |
| 1.00 | 6.98 | 0.18 | — | — | — | — | — |
| 0.80 | 7.70 | 0.10 | — | — | — | — | — |
| Transverse | | | | | | | |
| 0.40 | 2.70 | 0.07 | 2.93 | 0.05 | 2.90 | 0.05 | −0.20 |
| 0.50 | 3.40 | 0.08 | — | — | 3.63 | 0.04 | −0.23 |
| 0.60 | 4.01 | 0.07 | 4.20 | 0.06 | — | — | — |
| 0.70 | 4.64 | 0.05 | — | — | 4.93 | 0.04 | −0.29 |
| 0.80 | 5.20 | 0.10 | 5.38 | 0.04 | — | — | — |
| 0.90 | — | — | — | — | 6.00 | 0.04 | — |
| 1.00 | 6.14 | 0.07 | 6.33 | 0.03 | 6.45 | 0.05 | −0.31 |
| 0.90 | — | — | — | — | 6.88 | 0.05 | — |
| 0.80 | 6.90 | 0.09 | 6.95 | 0.06 | 7.15 | 0.06 | −0.25 |
| 0.60 | 7.25 | 0.10 | — | — | 7.56 | 0.05 | −0.31 |
| 0.40 | 7.57 | 0.10 | — | — | 7.63 | 0.10 | −0.06 |
| Longitudinal (lambda for B2 and BCC) | | | | | | | |
| 0.20 | — | — | 7.24 | 0.12 | 7.30 | 0.08 | |
| 0.40 | — | — | — | — | 7.25 | 0.14 | |
| 0.50 | — | — | — | — | 7.30 | 0.10 | |
| 0.20 | 6.88 | 0.10 | 6.58 | 0.12 | 6.20 | 0.07 | |
| 0.40 | — | — | — | — | 6.30 | 0.08 | |
| 0.50 | 6.70 | 0.11 | — | — | 6.45 | 0.12 | |
| 0.80 | 6.65 | 0.13 | — | — | — | — | |
| 1.00 | 6.68 | 0.12 | 6.72 | 0.18 | 6.75 | 0.08 | |
| Transverse (pi for B2 and BCC) | | | | | | | |
| 0.20 | 7.43 | 0.11 | 7.45 | 0.07 | 7.45 | 0.09 | −0.02 |
| 0.00 | 6.81 | 0.14 | — | — | 6.33 | 0.07 | 0.48 |
| 0.10 | — | — | — | — | 6.14 | 0.05 | — |
| 0.20 | 5.98 | 0.08 | 5.93 | 0.05 | — | — | — |
| 0.30 | 5.67 | 0.07 | 5.59 | 0.06 | 5.40 | 0.02 | 0.27 |
| 0.50 | 4.83 | 0.06 | 4.78 | 0.04 | 4.55 | 0.04 | 0.28 |
| 0.70 | 4.17 | 0.07 | 3.95 | 0.03 | 3.70 | 0.03 | 0.47 |
| 0.80 | 3.86 | 0.06 | 3.60 | 0.08 | — | — | — |
| 0.90 | — | — | — | — | 3.13 | 0.04 | — |
| 1.00 | 3.58 | 0.04 | 3.31 | 0.07 | 3.08 | 0.06 | 0.50 |

**Table 2.** Frequencies in THz ($\nu$) of [0$qq$] $D0_3$ and B2 modes, and corresponding [00$q$] and [$qq$2] BCC modes, as for table 1.

| | BCC | | B2 | | $D0_3$ | | BCC-$D0_3$ |
|---|---|---|---|---|---|---|---|
| $q$ | $\nu$ | Error | $\nu$ | Error | $\nu$ | Error | |
| Longitudinal | | | | | | | |
| 0.20 | 3.03 | 0.06 | 3.08 | 0.06 | 2.90 | 0.07 | 0.13 |
| 0.25 | — | — | — | — | 3.70 | 0.16 | — |
| 0.30 | 4.44 | 0.11 | 4.45 | 0.09 | 4.45 | 0.11 | −0.01 |
| 0.35 | — | — | — | — | 5.10 | 0.12 | — |
| 0.40 | 5.68 | 0.10 | 5.74 | 0.07 | 5.85 | 0.06 | −0.17 |
| 0.50 | 6.83 | 0.14 | 6.65 | 0.08 | 6.75 | 0.10 | 0.08 |
| 0.60 | 7.47 | 0.15 | — | — | 7.49 | 0.08 | −0.02 |
| 0.70 | — | — | — | — | 7.75 | 0.08 | — |
| Transverse 1 | | | | | | | |
| 0.30 | 2.93 | 0.05 | 3.09 | 0.04 | 3.13 | 0.05 | −0.20 |
| 0.40 | 3.80 | 0.03 | 3.90 | 0.03 | 4.05 | 0.03 | −0.25 |
| 0.50 | 4.62 | 0.07 | 4.76 | 0.03 | 4.85 | 0.03 | −0.23 |
| 0.60 | 5.30 | 0.04 | 5.41 | 0.09 | 5.49 | 0.03 | −0.19 |
| 0.70 | 5.83 | 0.07 | — | — | 6.05 | 0.05 | −0.22 |
| 0.80 | 6.24 | 0.08 | 6.30 | 0.08 | 6.40 | 0.07 | −0.16 |
| 0.90 | 6.50 | 0.11 | — | — | — | — | — |
| 1.00 | 6.68 | 0.12 | 6.72 | 0.18 | 6.75 | 0.08 | −0.07 |
| Transverse 2 | | | | | | | |
| 0.60 | — | — | 2.66 | 0.05 | 2.45 | 0.05 | — |
| 0.70 | 3.09 | 0.07 | 2.90 | 0.06 | 2.74 | 0.05 | 0.35 |
| 0.80 | 3.42 | 0.06 | 3.13 | 0.07 | 2.95 | 0.05 | 0.47 |
| 0.90 | 3.58 | 0.08 | — | — | — | — | — |
| 1.00 | 3.58 | 0.06 | 3.31 | 0.07 | 3.08 | 0.05 | 0.50 |
| Longitudinal (lambda for B2 and BCC) | | | | | | | |
| 0.40 | 7.20 | 0.08 | 7.25 | 0.08 | 7.23 | 0.04 | −0.03 |
| 0.50 | 6.72 | 0.09 | 6.55 | 0.12 | 6.40 | 0.06 | 0.32 |
| 0.60 | 6.00 | 0.08 | 5.93 | 0.17 | 5.71 | 0.06 | 0.29 |
| 0.65 | — | — | — | — | 5.26 | 0.09 | — |
| 0.70 | 5.14 | 0.10 | 5.08 | 0.17 | 4.86 | 0.05 | 0.28 |
| 0.75 | — | — | — | — | 4.35 | 0.05 | — |
| 0.80 | 4.42 | 0.09 | 4.22 | 0.08 | 3.95 | 0.05 | 0.47 |
| 0.90 | 3.76 | 0.09 | 3.58 | 0.07 | 3.28 | 0.07 | 0.48 |
| 1.00 | 3.58 | 0.04 | 3.31 | 0.07 | 3.08 | 0.06 | 0.50 |
| Transverse (pi for BCC) | | | | | | | |
| 0.00 | 7.60 | 0.07 | — | — | — | — | — |
| 0.20 | 7.63 | 0.13 | 7.58 | 0.15 | — | — | — |
| 0.50 | 7.33 | 0.08 | 7.43 | 0.10 | 7.61 | 0.08 | −0.28 |
| 0.80 | 6.83 | 0.10 | 6.95 | 0.11 | 7.15 | 0.09 | −0.32 |
| 1.00 | 6.68 | 0.12 | 6.72 | 0.18 | 6.75 | 0.08 | −0.07 |

Table 3. Frequencies in Thz ($\nu$) of [$qqq$] $D0_3$, B2 and BCC modes as for table 1.

| | BCC | | B2 | | $D0_3$ | | BCC-$D0_3$ |
|---|---|---|---|---|---|---|---|
| $q$ | $\nu$ | Error | $\nu$ | Error | $\nu$ | Error | |
| Longitudinal | | | | | | | |
| 0.15 | — | — | — | — | 2.95 | 0.08 | — |
| 0.20 | 3.81 | 0.04 | 3.89 | 0.08 | 3.90 | 0.06 | −0.09 |
| 0.30 | — | — | 5.55 | 0.09 | 5.55 | 0.07 | — |
| 0.40 | 6.69 | 0.12 | 6.80 | 0.10 | 6.70 | 0.07 | −0.01 |
| 0.45 | — | — | — | — | 7.10 | 0.07 | — |
| 0.50 | 7.47 | 0.10 | 7.48 | 0.18 | — | — | — |
| 0.50 | 7.47 | 0.10 | 7.48 | 0.18 | — | — | — |
| 0.20 | — | — | 7.85 | 0.09 | — | — | — |
| 0.10 | 7.33 | 0.12 | 7.40 | 0.06 | — | — | — |
| 0.05 | — | — | 7.20 | 0.12 | — | — | — |
| 0.00 | 6.81 | 0.14 | — | — | — | — | — |
| 0.00 | 6.81 | 0.14 | — | — | 6.33 | 0.07 | 0.48 |
| 0.05 | — | — | 6.50 | 0.11 | — | — | — |
| 0.10 | 6.05 | 0.08 | 6.05 | 0.05 | 5.75 | 0.11 | 0.30 |
| 0.20 | 5.43 | 0.09 | 5.38 | 0.10 | 5.08 | 0.09 | 0.35 |
| 0.30 | 5.00 | 0.09 | 4.95 | 0.08 | 4.78 | 0.06 | 0.22 |
| 0.40 | 5.35 | 0.12 | 5.17 | 0.14 | 5.00 | 0.07 | 0.35 |
| 0.45 | — | — | — | — | 5.31 | 0.07 | — |
| 0.50 | 6.05 | 0.12 | 5.90 | 0.12 | 5.65 | 0.06 | 0.40 |
| 0.50 | 6.05 | 0.12 | 5.90 | 0.12 | 5.65 | 0.06 | 0.40 |
| 0.45 | — | — | — | — | 6.08 | 0.07 | — |
| 0.40 | 6.60 | 0.16 | 6.64 | 0.12 | — | — | — |
| 0.35 | — | — | — | — | 6.92 | 0.06 | — |
| 0.30 | 7.28 | 0.11 | 7.30 | 0.08 | — | — | — |
| 0.20 | 7.55 | 0.10 | 7.55 | 0.13 | 7.55 | 0.18 | 0.00 |
| 0.10 | — | — | 7.65 | 0.09 | — | — | — |
| 0.00 | 7.60 | 0.11 | — | — | — | — | — |
| Transverse | | | | | | | |
| 0.30 | — | — | — | — | 2.53 | 0.12 | — |
| 0.40 | 3.25 | 0.08 | — | — | 3.35 | 0.08 | −0.10 |
| 0.50 | 4.10 | 0.10 | 4.14 | 0.09 | 4.10 | 0.08 | 0.00 |
| 0.50 | 4.10 | 0.10 | 4.14 | 0.09 | 4.10 | 0.08 | 0.00 |
| 0.40 | 4.80 | 0.15 | 4.78 | 0.09 | 4.73 | 0.07 | 0.07 |
| 0.30 | 5.42 | 0.11 | 5.45 | 0.06 | 5.35 | 0.06 | 0.07 |
| 0.20 | 5.86 | 0.12 | 5.85 | 0.10 | 5.70 | 0.11 | 0.16 |
| 0.10 | 6.35 | 0.15 | 6.24 | 0.09 | 6.00 | 0.08 | 0.35 |
| 0.05 | — | — | 6.48 | 0.14 | 6.20 | 0.09 | — |
| 0.00 | 6.81 | 0.14 | — | — | 6.33 | 0.07 | 0.48 |
| 0.00 | 6.81 | 0.14 | — | — | — | — | — |
| 0.10 | 7.15 | 0.14 | 7.18 | 0.16 | 7.28 | 0.12 | −0.13 |
| 0.20 | 7.32 | 0.14 | 7.35 | 0.09 | 7.41 | 0.07 | −0.09 |
| 0.30 | — | — | 7.40 | 0.09 | — | — | — |
| 0.40 | 7.53 | 0.14 | 7.53 | 0.09 | 7.58 | 0.07 | −0.05 |

$2\pi/A$ rather than the wave vector $2\pi/a$ of the BCC and B2 reciprocal lattices.

The major differences between the BCC and ordered curves (figure 2) are as follows:

(i) As discussed above, ordering causes a large increase in the frequencies of the highest frequency modes (here we rely on van Dijk's data).

(ii) The degenerate BCC [11$q$] $2\pi/A$ $\Lambda$ mode is split into two well-resolved modes for both B2 and $D0_3$. Van Dijk (1970) labelled these $\Delta_2'$ and $\Delta_1^{(2)}$ for $D0_3$.

(iii) There is a splitting of the [$qqq$] longitudinal and transverse mode at the origin of the $D0_3$ reciprocal lattice (the [111] $2\pi/A$ zone boundary for B2 and BCC). This is more apparent in the data for the [$qqq$] transverse modes. Robertson (1985) incorrectly identified [111] $2\pi/A$ as a $D0_3$ zone boundary.

(iv) There is a marked fall in the frequency of the soft transverse [$qq0$] mode as a result of ordering, and similar lowering of the adjoining curves [$qq2$] $2\pi A$ $\Lambda$ and [11$q$] $2\pi/A$ $\pi$ (denoted $\Sigma_1^{(1)}$ and $\Delta_5^{(1)}$ for $D0_3$ by van Dijk). The [$qq0$] mode becomes a zone boundary mode for the $D0_3$ structure when $q$ exceeds 0.75.

(v) The BCC [$qqq$] longitudinal mode has a minimum near $[\frac{4}{3}\frac{4}{3}\frac{4}{3}]$ $2\pi/A$. This minimum deepens further as the degree of order increases (but is indexed as $[\frac{2}{3}\frac{2}{3}\frac{2}{3}]$ $2\pi/A$ in B2 reciprocal space and as $[\frac{1}{3}\frac{1}{3}\frac{1}{3}]$ $2\pi/A$ in $D0_3$ reciprocal space).

Thus only a few of the expected splittings have actually been detected. Examination at greater resolution is required to detect the finer details. For $D0_3$ order there is some evidence of zone-boundary splitting for the low frequency [$qqq$] transverse modes ($\Lambda_3^{(1)}$ and $\Lambda_3^{(2)}$), and of splitting at a point where [$qq0$] acoustic and optic longitudinal modes ($\Sigma_1^{(1)}$ and $\Sigma_1^{(2)}$) come close to each other (and would be acoustic modes of the same frequency but of different phonon wave vectors for a BCC crystal). The neutron groups at these locations have the appearance of unresolved double peaks. Curves obtained from Born–von Karman models and drawn through the data points emphasize the splitting at such points (see e.g. van Dijk 1970).

No resonance effects were detected for the disordered crystal (See e.g. Kunitomi *et al* 1980, Kamitakahara and Brockhouse 1974, Tsunoda *et al* 1979). However, the neutron groups were significantly sharper for the fully ordered ($D0_3$) crystal. The average halfwidth for BCC was 1.30 times that for $D0_3$. For B2 (partially ordered) the average halfwidth was 1.16 times that for $D0_3$.

Measurements at high frequencies were difficult because of low intensities, especially for the (unfocused) longitudinal modes. This was particularly true of the [00$q$] L mode, for which the frequencies are little different from the transverse mode.

## 5. Born–von Karman models

The data for the three structures were analysed by fitting sixth-nearest neighbour Born–von Karman models as follows:

(i) Least squares curve fitting to a BCC model, using the mass of an 'average' atom, to obtain atomic force constant values for each of the three states of order (Robertson 1985). This indicated that most of the differences between the BCC, B2 and $D0_3$ results could be explained by changes in the $\alpha 2$ AFC.

(ii) Least squares curve fitting to the appropriate B2 or $D0_3$ model, using sublattice masses calculated from the order parameters listed in section 2. Van Dijk's data for $D0_3$ were also fitted.

Curve fitting to the B2 and $D0_3$ models showed that in addition to changes in $\alpha 2$, the nearest neighbour AFCs also undergo significant change as a result of ordering. These results are summarized in table 4. The different sets of results for the $D0_3$ crystal structure are discussed first, followed by a comparison of the AFC for different states of order.

### *5.1. $D0_3$ atomic force constants*

Van Dijk (1970) used a third-neighbour model to fit his experimental results, obtaining the AFCs listed in the final column of table 4 (column 6). In the current work, van Dijk's data have been modelled using a sixth-neighbour model in which the sublattice masses were calculated from each of the following sets of order parameters:

| | | |
|---|---|---|
| column 5 | $S_{11} = 0.50$ | $S_{31} = 1.00$ |
| column 4 | $S_{11} = 0.47$ | $S_{31} = 0.83$ . |

Column 5 of table 4 corresponds to perfect $D0_3$ order, and column 4 to the same degree of order as estimated for the $D0_3$ crystal used in the present study (possibly a more realistic situation than the perfect $D0_3$ order assumed by van Dijk).

As can be seen from table 4, the AFCs derived from van Dijk's data undergo significant changes as the number of neighbours in the model is increased and as the assumed state of order is changed. In the following discussion the AFCs in column 4 are regarded as those most appropriate to van Dijk's data.

The sets of AFC for the $D0_3$ crystals of the present work and of van Dijk (1970) in columns 3 and 4 of table 4 are very similar (both are based on $S_{31} = 0.83$ and $S_{11} = 0.47$). The major discrepancy is in the second nearest neighbour AFCs. The differences between the $\alpha 2$ and $\beta 2$ AFCs for Fe–Al and Fe–Fe atom pairs, $\alpha 2^{34} - \alpha 2^{12}$ and $\beta 2^{34} - \beta 2^{12}$, are larger for the current data than for van Dijk's data (5.1 and 2.4 compared with 4.7 and 0.9). This results from the greater separation of the $[00q]$ $\Delta_2'$ and $\Delta_1^{(2)}$ modes (Gilat and Dolling 1965). These modes arise from the splitting of the degenerate BCC $[11q]$ $2\pi/A$ $\Lambda$ mode.

### *5.2. Effect of degree of order on AFCs*

The effect of increasing degree of order on the sixth-nearest neighbour AFCs for the Fe–Al alloys of the present study may be seen by comparing columns 1, 2 and 3 of table 4. Fitting the BCC, B2 and $D0_3$ data to a BCC model indicated that the $\alpha 2$ AFC might be the most sensitive to changes in the degree of order (Robertson 1985). The full results (columns 1, 2, 3) confirm very large relative changes during ordering for the $\alpha 2^{12}$ and $\alpha 2^{34}$ AFC. However they also reveal significant changes for the $\alpha 1$, $\beta 1$ and $\beta 2$ AFCs. The most consistent trends are as follows:

(i) A notable feature is that the AFCs for Fe–Al (or Fe–Fe/Al) atom pairs are significantly higher than the corresponding AFCs for the Fe–Fe pairs. For example, $\beta 1^{14} >> \beta 1^{13}$ and $\alpha 2^{34} >> \alpha 2^{12}$. The difference increases as the degree of order increases.

(ii) The nearest neighbour AFCs exhibit a general increase, and the second neighbour AFCs a general decrease, as the degree of order increases. However this trend is masked to some degree by the changes noted in (i).

Consistent trends are not apparent in the AFC values for more distant neighbours.

Table 4. Atomic force constants in N $m^{-1}$.

| Model | BCC | B2 | $DO_3$ | | | |
|---|---|---|---|---|---|---|
| Column | 1 | 2 | 3 | 4 | 5 | 6 |
| at.% Al | 22.5 | 25 | 25 | 25 | 25 | 25 |
| Note | a | a | a | b | c | d |
| $\alpha 1^{13}$ | 12.2 | 13.7 | 13.1 | 13.3 | 14.5 | 14.69 |
| $\alpha 1^{14}$ | 12.2 | 13.7 | 19.0 | 19.3 | 18.0 | 17.78 |
| $\beta 1^{13}$ | 12.4 | 12.9 | 12.7 | 12.8 | 13.1 | 14.47 |
| $\beta 1^{14}$ | 12.4 | 12.9 | 18.9 | 18.9 | 18.3 | 19.14 |
| $\alpha 2^{12}$ | 7.1 | 5.2 | 1.1 | 1.5 | 1.3 | 2.10 |
| $\alpha 2^{34}$ | 7.1 | 5.5 | 6.2 | 6.2 | 6.1 | 5.87 |
| $\beta 2^{12}$ | 2.4 | 1.9 | 0.4 | 0.7 | 1.3 | 1.39 |
| $\beta 2^{34}$ | 2.4 | 2.2 | 2.8 | 1.6 | 0.1 | 0.19 |
| $\alpha 3^{11}$ | 1.9 | 2.5 | 1.3 | 1.3 | 1.5 | 1.42 |
| $\alpha 3^{33}$ | 1.9 | 0.6 | 1.5 | 1.4 | 1.55 | 1.46 |
| $\alpha 3^{44}$ | 1.9 | 0.6 | 0.5 | 0.6 | 0.5 | 0.31 |
| $\beta 3^{11}$ | −0.4 | −0.3 | −0.4 | −0.3 | −0.3 | |
| $\beta 3^{33}$ | −0.4 | −0.1 | −0.5 | −0.4 | −0.4 | |
| $\beta 3^{44}$ | −0.4 | −0.1 | −0.1 | −0.1 | 0 | |
| $\gamma 3^{11}$ | 2.1 | 1.2 | 0.8 | 0.7 | 0.8 | |
| $\gamma 3^{33}$ | 2.1 | 0.8 | 0.8 | 0.7 | 0.8 | |
| $\gamma 3^{44}$ | 2.1 | 0.8 | 0.6 | 0.6 | 0.4 | |
| $\alpha 4^{13}$ | 0.2 | 0.2 | 0.8 | 0.8 | 0.7 | |
| $\alpha 4^{14}$ | 0.2 | 0.2 | 0.9 | 0.9 | 0.8 | |
| $\beta 4^{13}$ | −0.3 | −0.8 | −0.3 | −0.3 | −0.3 | |
| $\beta 4^{14}$ | −0.3 | −0.8 | −0.4 | −0.5 | −0.5 | |
| $\gamma 4^{13}$ | 0 | 0.1 | −0.2 | −0.5 | −0.5 | |
| $\gamma 4^{14}$ | 0 | 0.1 | 0 | 0 | 0.1 | |
| $\delta 4^{13}$ | −0.2 | 0.1 | 0 | −0.05 | 0 | |
| $\delta 4^{14}$ | −0.2 | 0.1 | 0 | 0 | 0 | |
| $\alpha 5^{12}$ | 0.4 | 0.4 | 0.4 | 0.4 | 0.4 | |
| $\alpha 5^{34}$ | 0.4 | 0.5 | 0.4 | 0.4 | 0.45 | |
| $\beta 5^{12}$ | 1.0 | 0.4 | 0.4 | 0.9 | 0.8 | |
| $\beta 5^{34}$ | 1.0 | 0.5 | 0.5 | 1.0 | 0.9 | |
| $\alpha 6^{11}$ | −0.6 | −0.9 | −1.2 | −1.1 | −1.0 | |
| $\alpha 6^{33}$ | −0.6 | −0.5 | −1.0 | −0.9 | −0.9 | |
| $\alpha 6^{44}$ | −0.6 | −0.5 | −0.9 | −0.8 | −0.7 | |
| $\beta 6^{11}$ | −0.1 | 1.6 | −0.1 | 0 | 0.1 | |
| $\beta 6^{33}$ | −0.1 | 0.5 | 0 | 0 | 0.1 | |
| $\beta 6^{44}$ | −0.1 | 0.5 | −0.1 | −0.2 | −0.3 | |

[a] Present data.
[b,c] Van Dijk's data. Order parameters $S_{31} = 0.83$ $S_{11} = 0.47$ and $S_{31} = 1.0$ $S_{11} = 0.5$ respectively.
[d] Van Dijk's AFCs.

In the process of adjusting the AFCs to fit the data it was noted that the soft $[0qq]$ transverse mode is the low frequency phonon mode most sensitive to changes in the AFCs. Castan *et al* (1990) predicted that the corresponding $c'$ elastic constant would be the most sensitive to changes in the degree of order. The high frequency $D0_3$ modes at about 10 THz are also sensitive to the AFCs, but are also very sensitive to the effect that ordering has on the sublattice masses.

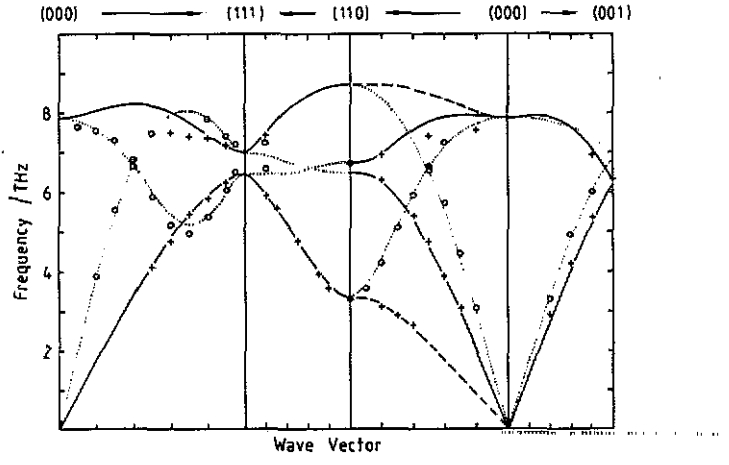


**Figure 3.** Phonon dispersion curves for B2-ordered Fe–Al ($D0_3$ indexing). Experimental points are denoted o for longitudinal modes and + for transverse modes. Born–von Karman curves for the AFCs shown in table 4 column 2 are shown as dotted lines for longitudinal modes and dashed or full lines for transverse modes.

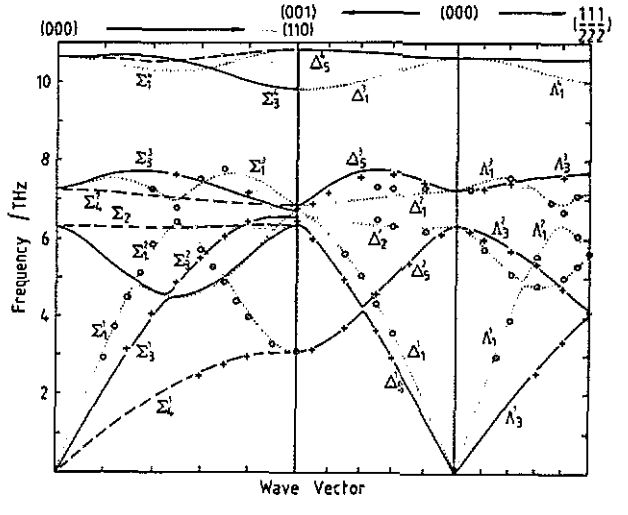


**Figure 4.** Phonon dispersion curves for $D0_3$-ordered Fe–Al (*as for figure 3 except* that the AFCs are from table 4, column 3).

## 6. Conclusion

The experimental dispersion curves for BCC-, B2- and $D0_3$-ordered Fe–Al alloys are very similar (except at very high frequencies). However, the differences are much more pronounced than those previously reported for other alloys in ordered and disordered states ($Cu_3Au$ and FeCo). This is only to be expected in view of the large differences in size, mass and electron structure of the iron and aluminium atoms. The phonon frequencies generally follow a consistent trend through the ordering sequence BCC to B2 to $D0_3$, and some of the expected zone-boundary splittings have been detected. The data obtained for $D0_3$-ordered $Fe_3Al$ in the present study are in good agreement with those obtained previously by van Dijk (1970).

Born–von Karman modelling shows that ordering causes:

(i) Large relative change in the second-neighbour atomic force constants.

(ii) Much larger values of the AFCs for Fe–Al atom pairs than of the corresponding AFCs for Fe–Fe atom pairs (first and second neighbours only).

The low frequency phonon mode most sensitive to changes in the AFC is the soft transverse [$qq$0] mode, of great interest in relation to martensitic transformations and ordering kinetics (Vennegues *et al* 1990).

## Acknowledgments

The author gratefully acknowledges the award of a Fellowship by the Australian Institute of Nuclear Science and Engineering and the assistance of the staff of the Metallurgy Department, University of Newcastle, and Neutron Diffraction Group, Lucas Heights.

## References

Borgonovi G, Logiudice G and Tocchetti D 1967 *J. Phys. Chem. Sol.* **28** 467
Bradley A J and Jay A H 1932 *Proc. R. Soc.* A **136** 210
Brockhouse B N 1966 *Phonons* ed RWH Stevenson (Edinburgh: Oliver and Boyd) p 110
Brockhouse B N, Hallman E D and Ng S C 1967 *Magnetic and Inelastic Scattering of Neutrons by Metals* ed T J Rowland and P A Beck (New York: Gordon and Breach) p 163
Castan T, Vives E and Planes A 1990 *J. Phys.: Condens. Matter* **2** 1743
Flinn P A, McManus G M and Rayne J A 1960 *J. Phys. Chem. Sol.* **15** 189
Gilat G and Dolling G 1965 *Phys. Rev.* A **138** 1053
Guttman L, Schnyders H C and Arai G J 1969 *Phys. Rev. Lett.* **22** 517
Hallman E D 1974 *Can. J. Phys.* **52** 2235
Hallman E D 1976 *Bull. Am. Phys. Soc.* **21** 368
Kamitakahara W A and Brockhouse B N 1974 *Phys. Rev.* B **10** 1200
Koster W and Godecke T 1980 *Z. Metall.* **71** 765
Kunitomi N, Tsunoda Y and Shiraishi H 1980 *Solid State Commun.* **34** 519
Leamy H J, Gibson E D and Kayser F X 1967 *Acta Metall.* **15** 1827
Nicklow R M 1979 *Treatise on Materials Science and Technology* vol 15, ed G Kostorz (New York: Academic) p 191
Okamoto H and Beck P A 1971 *Metall. Trans.* **2** 569
Oki K, Hasaka M and Eguchi T 1973a *Japan. J. Appl. Phys.* **12** 1522
—— 1973b *Trans. Japan. Inst. Met.* **14** 8
—— 1977 *Trans. Japan. Inst. Met.* **18** 750
Owen W S 1990 *Mater. Sci. Eng.* A **127** 197

Robertson I M 1985 *Solid State Commun.* **53** 901
Robinson R A, Squires G L and Pynn R 1984 *J. Phys. F: Met. Phys.* **14** 1061
Rudman R S 1960 *Acta Metall.* **8** 321
Smith A W and Rawlings D 1976 *Phys. Status Solidi* A **34** 117
Swann P R, Duff W R and Fisher R M 1972 *Metall. Trans.* **3** 409
Taylor A and Jones R M 1958 *J. Phys. Chem. Sol.* **6** 16
Tsunoda Y, Kunitomi N, Wakabayashi N, Nicklow R M and Smith H G 1979 *Phys. Rev.* B **19** 2876
Turchi P, Calvayrac Y and Plique F 1978 *Phys. Status Solidi* A **45** 229
van Dijk C 1970 *Phys. Lett.* **32A** 255
Vasil'kevich A A 1981 *Metallofizika* **3** 55
Venkataraman G, Feldkamp L A and Sahni V C 1975 *The Dynamics of Perfect Crystals* (Cambridge, MA: MIT Press)
Vennegues P, Cadeville M C, Peirron-Bohnes V and Afyouni M 1990 *Acta Metall.* **38** 2199